Texture Analysis of Sidescan Sonar Imagery Using Statistical Scattering Models

Hugh Griffiths, Jonathan Dunlop and Roger Voles

Department of Electronic and Electrical Engineering
University College London
Torrington Place, London, WC1E 7JE, UNITED KINGDOM
Email: h.griffiths@eleceng.ucl.ac.uk

Abstract

It is shown that the generalised K-distribution provides a good fit to the amplitude statistics of sonar imagery from several different types of seabed sediment. A number of possible explanations for the Ricean nature of the speckle component have been put forward. A method of refining the estimated position of a sediment boundary using maximum likelihood is also presented.

1. Introduction

In the analysis of high-resolution sonar imagery of the seabed, it is important to properly model the image texture in order to be able to detect objects that do not conform to this model. The K-distribution can be used to model the amplitude statistics of a coherent imaging process, and has been applied in the past to high-resolution maritime radar clutter and SAR imagery of land scenes. Oliver [1] demonstrated that a single sonar image of sand ripples followed the K-distribution, but it does not appear to have been applied to a full range of seabed sediment types. Sonar images from several different types of sediment are described in section 2, and the single point statistics of this data is investigated in section 3. A model-based segmentation of a sonar image will be unpredictable where the sample window crosses a sediment boundary, so a method of refining the estimate of the boundary position using maximum likelihood is presented in section 4. The work is summarised in section 5.

2. Sidescan sonar data

Data from two sidescan sonar systems over a wide range of sediments are considered. Both data sets contain amplitude returns quantised to 8-bits, but no phase information was recorded.

Five sonar images from homogeneous regions of stones, gravel, sand, clay and mud from the ground-truthed data set of Pace and Gao [2] are used. These were acquired with a 48kHz centre frequency, 2kHz bandwidth system with a resolution cell of approximately 38cm/2.2m in the across/along track directions. Each of the images was normalised to fill the quantisation range and some contain DC offsets.

The second data set is a 100kHz image from the work in [3] which contains regions of sand, gravel and gravel ripples that were identified from camera footage and grab-sampling. The resolution cell was approximately 20cm in both directions. The change of grazing angle within each image did not appear to alter the local image statistics, so a histogram of the whole sediment region was used for distribution fitting.

3. Statistical scattering models

The physical processes involved in radar backscatter are well understood and statistical models incorporating these processes have been widely used in radar signal processing.

3.1 Rayleigh distribution

The echo of a radar or sonar pulse can be considered to be the sum of contributions from N discrete scattering centres existing within the resolution cell.

$$S = \sum_{n=1}^{N} a_n \exp(j\phi_n) \tag{1}$$

where a_n and ϕ_n represent the amplitude and phase shift of the nth contribution. The randomly phased returns may interfere constructively or destructively, so the amplitude $|S|$ will fluctuate from cell to cell. It is usually assumed that: (i) a_n and ϕ_n are statistically independent random variables; (ii) the positions of the scatterers are sufficiently random to introduce path differences greater than the incident wavelength, so the distribution of ϕ_n can be considered uniform over 2π; (iii) all the contributions are at the same frequency; and (iv) N is large, so the Central Limit Theorem can be applied. Re(S) and Im(S) are then both zero-mean Gaussian, which leads to Rayleigh distributed amplitude $|S|=x$

$$p(x) = \frac{2x}{\overline{a^2}} \exp\left(\frac{-x^2}{\overline{a^2}}\right) \tag{2}$$

where $\overline{a^2}$ is the mean-square of step-lengths a_n.

3.2 K-distribution

At high resolution, spatial structure on the seafloor such as sediment ripples is resolved and N varies from cell to cell. This bunching of scatterers is represented by a spatially varying mean level that modulates the Rayleigh 'speckle' component. The underlying component was found to be an empirical, but good fit to the gamma distribution in maritime radar clutter and SAR images. Combining these two components results in the K-distribution for overall amplitude [4]. This converges to the Rayleigh as $\nu \to \infty$

$$p(x) = \frac{2b}{\Gamma(\nu)}\left(\frac{bx}{2}\right)^{\nu} K_{\nu-1}(bx) \tag{3}$$

where $b^2 = \frac{4\nu}{\overline{a^2}}$ (4)

ν is the shape parameter that characterises scatterer bunching, $K_{\nu-1}$ is a modified Bessel function of order ν-1. The particular value of this model is that it can also model all the spatial correlation properties of the texture [1]. A numerical search was used to obtain the least-squares fit of the distribution to the eight sediment histograms and the results are shown in figure 1. A DC offset was included as a search parameter for the 48kHz data.

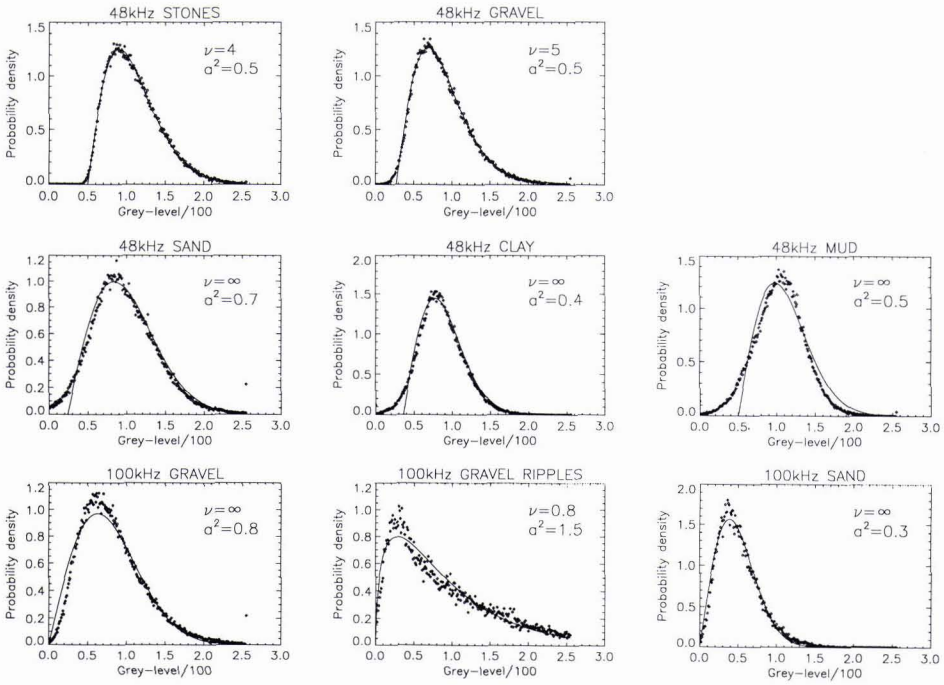

Figure 1: Least-squares fits of K-distribution to data

The K-distribution provided a good fit to sonar data from large particles such as stones and gravel, but the probability density function (PDF) of a very fine sediment like mud resembled a Gaussian distribution with a non-zero mean, and the K-distribution provided a poor fit Other sediments had PDFs between these extremes. The gravel ripples had a very low value of ν indicating large variations in the underlying model.

3.3 Generalised K-distribution

The Ricean distribution [5] results from the envelope detection of a steady sinusoidal signal plus zero-mean Gaussian noise, and reduces to the Rayleigh and non-zero-mean Gaussian distributions in limiting cases. The PDFs of the fine sediments suggest that the Ricean may be a more suitable model for the speckle statistics than the Rayleigh.

If Ricean speckle is modulated by an underlying gamma distribution, the received signal will follow the generalised K-distribution [6].

$$p(x)=\frac{2b}{\Gamma(\nu)}\left(\frac{4\nu x}{b\overline{a^2}}\right)^{\nu} I_0\left(\frac{2\delta x}{\overline{a^2}}\right)K_{\nu-1}(bx) \qquad (5)$$

$$\text{where } b^2=\frac{4\nu}{\overline{a^2}}+\frac{4\delta^2}{\left(\overline{a^2}\right)^2} \qquad (6)$$

δ is the amplitude of the non-random contribution, and I_0 is a modified Bessel function of zero order. Figure 2 shows the generalised K-distribution fitted to the data.

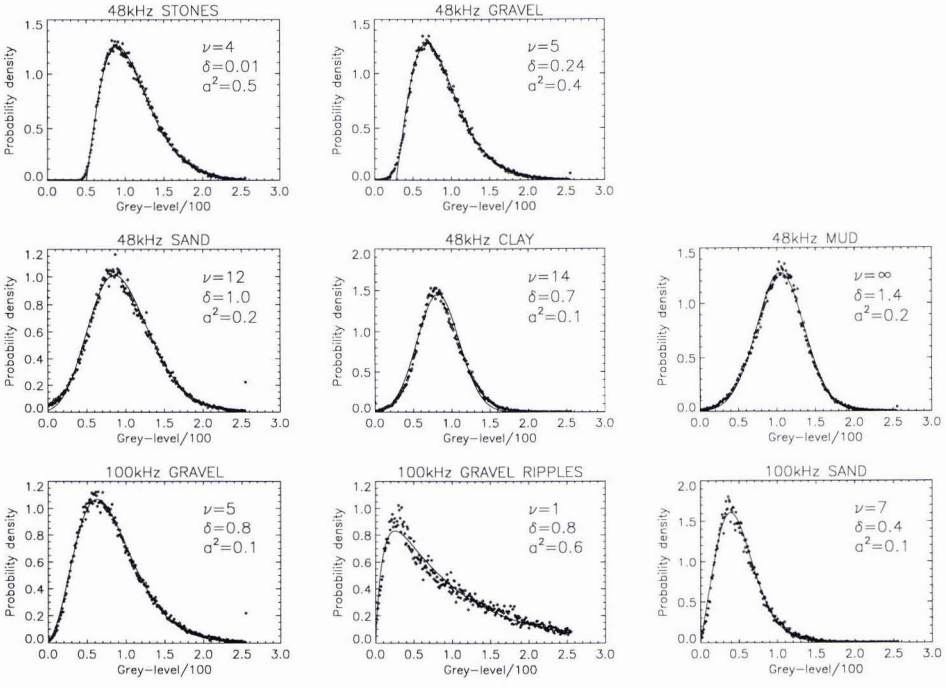

Figure 2: Least-squares fits of generalised K-distribution to data

The generalised K-distribution is an excellent fit to all of the wide range of sediments tested. There is generally more structure visible in the data of sediments with large particle size like stones than fine sediments like mud, subsequently ν tends to decrease with particle size.

A small tail at low amplitudes is visible in the 48kHz data of stones and gravel that is not modelled by the generalised K-distribution. The return signal envelope was recorded in analogue form on magnetic tape [2] which could add zero-mean Gaussian noise to the data. A signal-to-noise ratio of 20dB provides a tail of the magnitude observed in the gravel data and may be a plausible explanation. The tail was ignored in the fitting of distributions, but its existence precluded the use of Kolmogorov-Smirnov or χ^2 statistics, so the mean-square fit was used instead.

There are a number of possible causes of the Ricean speckle:-

(i) Acoustic energy penetrates the sediment and a single specular echo is received from a gas-rich sub-bottom sediment layer [7] or the underlying rock layer.

(ii) The sonar equipment adds a small, constant amplitude signal such as transmitter breakthrough to the received signal before envelope detection. Ricean statistics may be observed from other sidescan sonar systems [8], so this effect is not due to a single piece of faulty equipment. The amplitude of the contribution δ would be constant for all sediments but as the 48kHz data was normalised the parameter δ would tend to zero for strongly backscattering sediments such as stones and gravel, as observed in the data.

(iii) The resolution cell contains a fine sediment with a single stone that gives a strong contribution. Any cells containing 2 or 3 specular reflectors would give non-Ricean returns [9] and an even greater number would produce approximately Rayleigh statistics.

(iv) Small ripples within the resolution cell of equal wavelength to the sonar generate a Bragg resonant effect. This phenomenon is unlikely to occur in all of the images tested

(v) Reverberation from the sonar-bottom-surface-bottom-sonar path with the same delay as the main backscatter. The reverberation would be a random variable and the variance may preclude its simplification to a constant.

(vi) Re(S) and Im(S) were Gaussian with non-zero mean, due to a non-uniform distribution of ϕ_n. The 48kHz sonar had λ ~3cm and range resolution~38cm which gives 12 cycles within the resolution cell at grazing incidence. This should provide sufficient phase run out to ensure a fairly uniform phase distribution.

(vii) The fractional bandwidth of sidescan sonar is much greater than radar, so the assumption of monochromatic speckle in section 3.1 may not hold. The intensity distribution arising from polychromatic laser light or light of finite bandwidth becomes the sum of correlated monochromatic speckle patterns. As the correlation increases there is a transition from Rayleigh distributed amplitude towards a delta function centred at the r.m.s. amplitude [10]. The complexity of the exact PDF makes it computationally unattractive, but the Ricean distribution exhibits very similar behaviour.

3.4 Comparison of distributions

The Weibull and lognormal distributions are empirical distributions that are often used to model radar clutter and have previously been applied to sonar data [11]. These were tested against the Rayleigh, K-distribution, Ricean and generalised K-distributions to determine which modelled the data most accurately. The mean-square difference between the PDFs of the sediment and the candidate distribution are shown in table 1.

	48kHz data					100kHz data			
	Stones	Gravel	Sand	Clay	Mud	Gravel	Ripples	Sand	Overall
Rayleigh	2.29	2.20	2.94	4.60	10.1	4.56	52.3	4.25	10.41
K-dist	0.58	0.89	2.94	4.60	10.1	4.56	4.27	4.22	4.02
Ricean	2.29	2.20	2.36	2.79	1.11	3.83	52.3	4.25	8.89
Weibull	0.82	1.54	2.02	2.81	1.15	2.64	6.28	3.90	2.65
Lognormal	1.08	0.50	0.98	1.18	2.14	2.26	2.89	5.82	2.11
Gen K-dist	0.58	0.89	0.96	1.40	1.11	2.76	2.64	2.76	1.37

Table 1: Mean-square difference between model and sediment PDFs ($x10^{-3}$). The best fit in each col. is shaded.

The generalised K-distribution offers the best fit to the data and the lognormal also fits well despite having one less parameter. The advantage of the generalised K-distribution is that it will also model all the spatial correlation properties of the texture.

A statistical model can be used to segment sonar imagery into regions of different sediments. A small sample window is passed across the image and the parameters of the statistical model are estimated. The central pixel of the window is then classified on the basis of these estimated parameters. The even order moments of the generalised K-distribution are given in [6] which could be used for parameter estimation, but with three parameters the 2nd, 4th and 6th moments of the data would be required. The 6th moment would not be a robust estimator unless a very large sample window was used. It is not possible to derive a maximum likelihood estimate analytically for the K-distribution, but Oliver derived a good approximation in [12]. It may be possible to do the same with the generalised K-distribution.

4. Maximum likelihood boundary estimator

As the sample window crosses a sediment boundary the samples will follow a mixture distribution and classification errors will result as shown in figures 3 and 4. The estimate of the boundary position could then be refined if two adjacent sample windows were passed across the boundary.

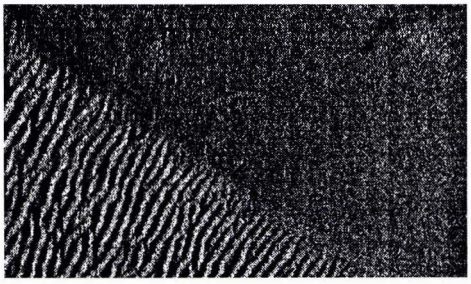

Figure 3: Section of 48kHz image

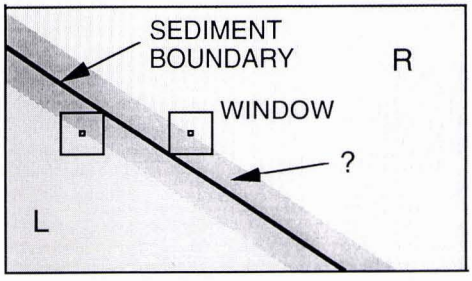

Figure 4: Classification map of figure 3

Suppose that the probability distributions of the amplitude x in the areas L and R are P_L and P_R respectively.

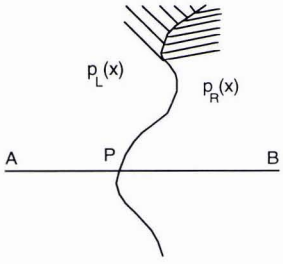

Figure 5: Sediment boundary

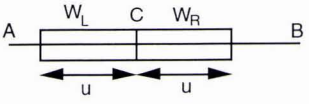

Figure 6: Sample windows

By scanning along the line AB shown in figure 5, it is required to determine the position P of the intersection of the boundary with the line. Consider two contiguous windows W_L and W_R as shown in figure 6, each comprising u adjacent pixels lying along the line AB and abutting at the point C.

The likelihood L that the contents of the u pixels, ω_L, in W_L all coming from the LH distribution is

$$L = \prod_{\omega_L} p_L(x) \tag{7}$$

When W_L is fully immersed in the LH area, the expected value of L will be $\overline{L_L}$, and when fully immersed in the RH area it will be $\overline{L_R}$. Clearly, $\overline{L_L} > \overline{L_R}$. Similarly, for W_R,

$$R = \prod_{\omega_R} p_R(x) \tag{8}$$

with $\overline{R_R} > \overline{R_L}$. Their relationships are shown in figure 7.

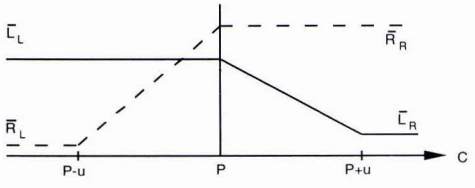

Figure 7: Likelihood as windows cross boundary P

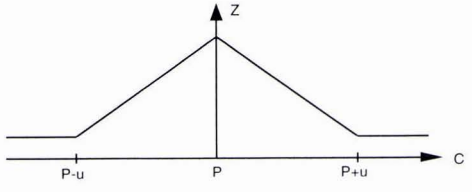

Figure 8: Joint likelihood as windows cross boundary P

It is evident that Z=LR will have an expected maximum when C lies on P as shown in figure 8.

An alternative arrangement would also take into account the degree of 'mismatch' between P_L and P_R, giving

$$L' = \prod_{\omega_L} \frac{p_L(x)}{p_R(x)} \qquad (9)$$

$$R' = \prod_{\omega_R} \frac{p_R(x)}{p_L(x)} \qquad (10)$$

These techniques were applied to the sonar image in figure 3. The K-distribution fits from section 3.2 were used for P_L and P_R, and u was arbitrarily chosen as 40 pixels. The likelihood L' and R' are shown in figures 9 and 10 with high intensity indicating high likelihood. These gave better performance than L and R which are not shown.

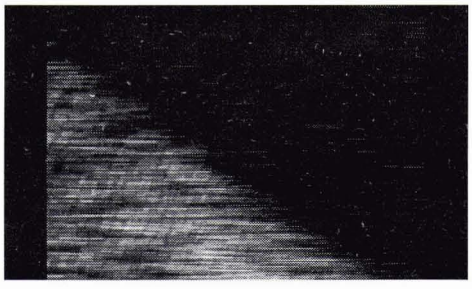

Figure 9: log L'

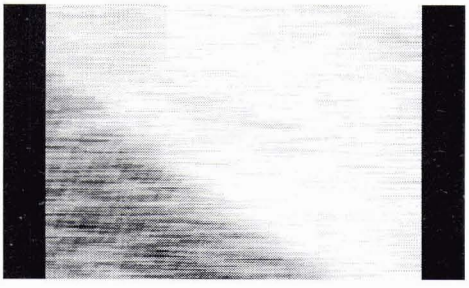

Figure 10: log R'

Figure 11 shows the combined likelihood Z'. A light strip indicating the most likely position of the sediment boundary is visible, but there is a lot of noise within the rippled region that would prevent accurate detection of the boundary.

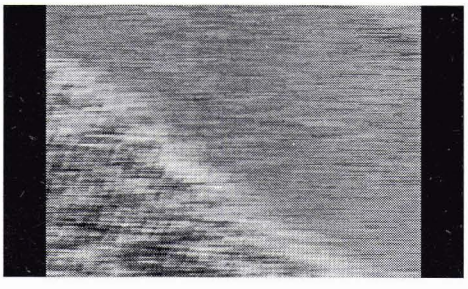

Figure 11: log Z'=log L'+log R'

It is known a priori that a particular row of L' should resemble the profile in figure 7. For every point c, $\overline{L'_L}$ was calculated from the mean of {u<L'<c} and $\overline{L'_R}$ from the mean of {c+u<L'<max(c)-u}. This profile was then tested against L' and the mean-square difference between the two was found. The value of c that minimised this difference should coincide with P. The optimum profile from row 83 of L' is shown in figure 12, and similarly for R' in figure 13. c=200 in both figures, which agrees with the visually estimated boundary in this row..

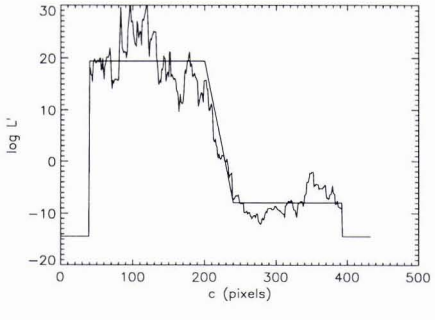

Figure 12: Row 83 of L' with optimum profile

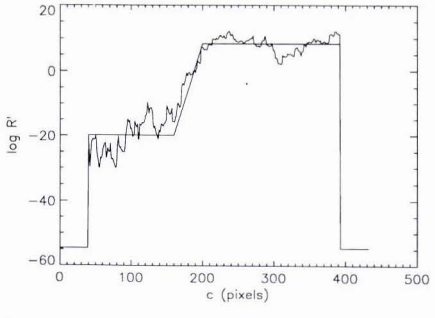

Figure 13: Row 83 of R' with optimum profile

Fitting these profiles on a row-by-row basis has the effect of filtering the likelihoods L' and R'. The filtered likelihoods are shown in figures 14 and 15.

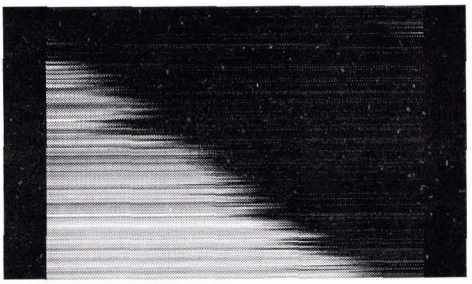

Figure 14: Filtered log L'

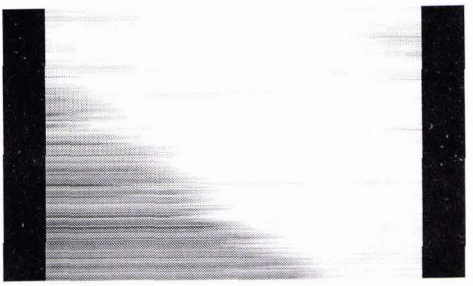

Figure 15: Filtered log R'

Comparison of figures 16 and 11 shows that filtering Z' improves the estimate of the boundary position.

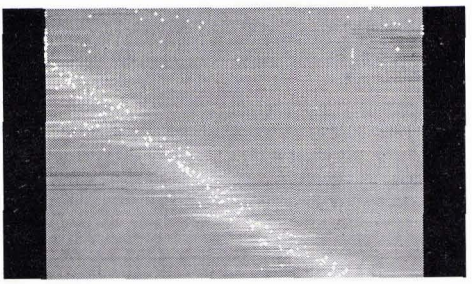

Figure 16: Filtered log L'+Filtered log R' with maxima

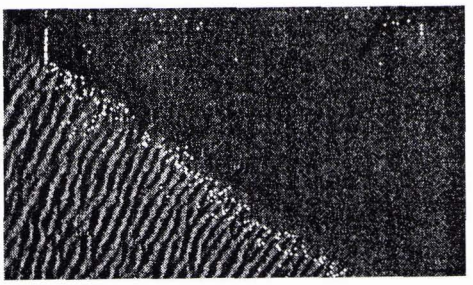

Figure 17: Maxima overlaid onto image

These results were achieved with W_L and W_R having a width of only one pixel. By orienting the search line AB perpendicular to the local boundary, W_L and W_R can have a greater width without sampling both distributions when positioned on the boundary (when C=P). It is proposed that the boundary estimate be represented as a number of linked nodes N. Each node N_i would then search along the normal defined by its neighbours N_{i-1} & N_{i+1} with chevron shaped W_L and W_R as shown in figure 18. These adaptations should allow the boundary estimator to iteratively converge onto a sediment boundary of any shape.

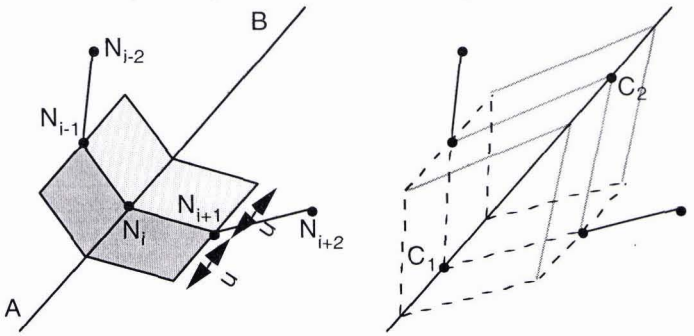

Figure 18: Chevron shaped windows searching perpendicular to local boundary estimate

5. Summary:

The K-distribution has been applied to sidescan sonar data, but poor agreement was found with sand and finer sediments. Modelling the speckle component with a Ricean distribution leads to the generalised K-distribution which provides a good fit to sonar imagery from several different types of seabed sediment. A number of possible explanations for the Ricean nature of the speckle component have been put forward. The lognormal also fits the data well but, unlike the generalised K-distribution, the lognormal will not model the spatial

correlation properties of the data.

A model-based segmentation of a sonar image will be unpredictable where the sample window crosses a sediment boundary. The statistics of the sediment on either side of the boundary are known, so two adjacent windows are passed across the boundary and maximum likelihood used to improve the estimated boundary position.

6. Acknowledgements

This work is supported by the Engineering and Physical Sciences Research Council and by DRA Bincleaves. We would like to thank R. Benjamin and K. Milne (visiting professors at UCL), Dr. D.R. Carmichael and Mr. G.J. Heald (DRA Bincleaves) and Prof. C.J. Oliver (DRA Malvern) for invaluable advice and discussions. We would also like to thank Dr. N.G. Pace for kindly supplying a set of the data from his work in [2].

References

[1] C.J. Oliver, "The interpretation and simulation of clutter textures in coherent images", *Inverse Problems*, vol. 2, pp.481-518, 1986

[2] N.G. Pace and H. Gao, "Swathe seabed classification", *IEEE J. Oceanic Eng.*, vol. OE-13, pp.83-90, 1988

[3] D.R. Carmichael, L. M. Linnet and S.J. Clark, "A multi-resolution directional operator for sidescan sonar image analysis", *J. Defence Science*, vol. 1, pp.453-459, 1996

[4] E. Jakeman and P.N. Pusey, "A model for non-Rayleigh sea echo", *IEEE Trans.* AP-24, pp. 806-814, 1976,

[5] S.O. Rice, "Mathematical analysis of random noise", *Bell Syst. Tech. J.*, vol.23, pp.282-332 & vol.24, pp.46-156

[6] E. Jakeman and R.J.A. Tough "Generalized K distribution: a statistical model for weak scattering", *J. Opt. Soc. Am.*, vol. 4, pp.1764-1772., 1987

[7] D. Tang, G. Jin, D.R. Jackson and K.L.Williams, "Analyses of high-frequency bottom and subbottom backscattering for two distinct shallow water environments", *J. Acoust. Soc. Am.*, vol. 96, pp.2930-2936, 1994,

[8] G. Shippey, A. Bolinder and R. Finndin, "Shade correction of side-scan sonar imagery by histogram transformation", *IEEE Oceans '94 Proceedings*, vol. 2, pp.439-443, 1994

[9] J.K. Jao and M. Elbaum, "First-order statistics of a non-Rayleigh fading signal and its detection", *Proc. IEEE*, vol. 66, pp.781-789, 1978

[10] G. Parry, "Some effects of temporal coherence on the first order statistics of speckle", *Optica Acta*, vol. 21, pp.763-772, 1974

[11] M. Gensane, "A statistical study of acoustic signals backscattered from the sea bottom", *IEEE J. Oceanic Eng.*, vol. 14, pp.84-93 1989

[12] C.J. Oliver, "Optimum texture estimators for SAR clutter", *J. Phy. D: Appl. Phys.*, vol. 26, pp.1824-1835, 1994